

Lateral Diffusion of Molecules in Two-Component Lipid Bilayer: A Monte Carlo Simulation Study

István P. Sugár^{*,†} and Rodney L. Biltonen[‡]

Graduate School of Biological Sciences, Mount Sinai School of Medicine, New York, New York 10029, and Departments of Pharmacology and Biochemistry & Molecular Genetics, University of Virginia Health Sciences Center, Charlottesville, Virginia 22908

Received: September 23, 2004; In Final Form: January 21, 2005

Lateral diffusion of membrane components makes possible any in-plane membrane reaction and has a key role in signaling in cell membranes. In this report the equilibrium lateral diffusion of intrinsic molecules in an equimolar DMPC/DSPC mixture is simulated using a thoroughly tested two-state model of two-component phospholipid bilayers. The model has been successful in calculating the excess heat capacity function, the most frequent center-to-center distances between DSPC clusters, and the fractal dimensions of gel clusters (Sugár, I. P., Thompson, T. E., Biltonen, R. L. *Biophys. J.* **1999**, 76, 2099–2110). In the gel/fluid mixed phase region, a diffusing intrinsic molecule may change its state from fluid to gel (or from gel to fluid) at any time. A common characterization of the diffusion of intrinsic molecules is given by the simulated average first-passage time curves. We find that these curves can be described as power functions containing two parameters, α and β , except near the percolation threshold of gel/fluid or compositional clusters. We find also that the intrinsic molecules are involved in approximately normal diffusion, i.e., $\beta \approx 2$ in the extreme gel and fluid phase regions, while in the gel/fluid and gel/gel mixed phase regions the diffusion is anomalous, i.e., $\beta \neq 2$. In the mixed phase regions, when the initial local state of the diffusing molecule is not specified, each component is involved in sub-diffusion ($\beta > 2$). In the gel/fluid mixed phase region molecules situated initially inside a fluid cluster are involved in sub-diffusion, but DMPC molecules situated initially inside a gel cluster are involved in super-diffusion ($\beta < 2$). The possibility of anomalous diffusion in membranes apparently arises because the diffusing molecule visits a variety of different environments characterized by its relative proximity to various membrane components. The diffusion is actually anomalous when the components of the bilayer are nonrandomly distributed. The deviation from random distribution is strongly correlated with β . Similar to the results of the NMR experiments, the calculated relative diffusion coefficient continuously decreases in the gel/fluid mixed phase region with decreasing temperature. In apparent contradiction, diffusion measured by fluorescence recovery after photobleaching (FRAP) demonstrates the existence of a threshold temperature, below which long-range diffusion of FRAP probe molecules is essentially blocked. This threshold temperature is highly correlated with the percolation temperature of gel clusters.

Introduction

The lateral diffusion of membrane components is of key importance in physiological processes in cells. Electron transfer in mitochondria^{1,2} and chloroplasts³ requires diffusion of mobile redox carriers. Lateral diffusion of membrane components is important in cell adhesion.^{4–6} Aggregation of membrane receptors can be important. Histamine release by mast cells is triggered by the aggregation of Fc receptors for IgE.^{7,8} The first steps in the action of insulin, epidermal growth factor, and nerve growth factor are the binding of hormone to its receptor and the cross-linking of the receptors.^{9–11}

Lateral motion of membrane components (reviewed by Toccane et al.¹² and Saxton¹³) is measured at different time and length scales depending on the technique. Shin et al.¹⁴ described an ESR technique permitting measurement of short-range and long-range diffusion coefficients in the same experiment on the same sample employed (ESR techniques are reviewed by Freed¹⁵). Fluorescence quenching and excimer formation are

short-range measurements in which the range is set by the distance a particle can diffuse during the fluorescence lifetime.^{16,17} However, the use of labels with long lifetimes extends the range significantly.^{18,19} Longer range measurements include: fluorescence recovery after photobleaching (FRAP),^{20–23} single particle tracking,²⁴ fluorescence resonance energy transfer (FRET),^{25,26} imaging fluorescence correlation spectroscopy,^{27,28} laser tweezers measurements,^{29,30} and barrier-free path measurement.^{31–33} In the experiments listed above the diffusion of a probe molecule is measured. Since the probe molecules can disturb the local membrane structure and preferentially exist in fluid-phase regions, the obtained diffusion coefficients do not necessarily reflect the diffusion properties of intrinsic membrane components, which may change from fluid to gel or from gel to fluid state at any time.

Quasielastic neutron scattering (QENS) and NMR are the only methods that do not require any labeling. However, the application of QENS is restricted due to large substance requirements and limited neutron beam time.³⁴ Thus, NMR remains as the only potentially label free method to study lateral diffusion in lipid bilayers and the only source of experimental

* Corresponding author.

[†] Mount Sinai School of Medicine.

[‡] University of Virginia Health Sciences Center.

TABLE 1: Lateral Diffusion Parameters of Intrinsic Molecules of One-Component Lipid Bilayers^a

| lipid | $T_c(K)$ | $D_L(u)$ | $\ln A$ | $E_a(kcal/mol)$ | phase | ref |
|-------|----------|----------|---------|--------------------------------------|------------|-----------|
| DLPC | 304 | 7.3 | -0.97 | 9.4 ± 0.2 | L_α | 35 |
| DMPC | 304 | 3.2 | 7.83 | 15.2 ± 0.3 | L_α | 35 |
| DPPC | 320 | 5 | 7.00 | 15.2 ± 0.2 (13.1 ± 0.1) | L_α | 35 |
| DSPC | 330 | | 6.2* | $15.2 \pm 0.2^*$ | L_α | estimated |
| DMPC | 295.5 | 0.02 | 38.58 | 36 | L_β | 65 |
| DPPC | 298 | 0.016 | 37.85* | 36* | L_β | 36 |
| DSPC | 298 | | 37.12* | 36* | L_β | estimated |

^a The diffusion coefficient $D_L(= A \cdot \exp[-E_a/RT])$ and the preexponential factor A are given in units $u = 10^{-8} \text{ cm}^2/s$. The diffusion coefficients for gel phase DMPC bilayers were taken from FRAP measurements,⁶⁵ because this is the only data available to estimate the activation energy, E_a in gel phase. The fluid phase data listed above refer to constant hydration of 20% D_2O (w/w). With increasing hydration E_a decreases slightly and levels off at 30% D_2O (w/w) (see the value in parentheses for DPPC). The data for DSPC are estimated based on the trend of the experimental data for DMPC and DPPC (marked by asterisk in Table 1).

data to compare with our simulations on lateral diffusion of intrinsic lipid molecules. By using pulsed gradient proton NMR spin-echo techniques Kuo and Wade³⁵ measured the long-range diffusion constant of the lipid molecules in fluid, one-component oriented phospholipid multilayers. Crawford et al.³⁶ were able to measure the diffusion constant in the gel phase of DPPC multilamellar vesicles by using combined multiple pulse and multiple pulse gradient proton NMR techniques. The experimental and estimated parameters of lateral diffusion are listed in Table 1.

Diffusion of a tracer in a heterogeneous membrane has been modeled using percolation theory or the theory of anomalous diffusion.^{37,38} In those models the diffusion of a point particle is considered as immobile obstacles are added at random. Initially, diffusion is unhindered. As obstacles are added, diffusion is increasingly hindered, until the percolation threshold is reached, i.e., when an infinite cluster of obstacles form. Above the threshold, long-range diffusion is blocked but local diffusion within finite domains is still possible.

Monte Carlo simulations are available for various obstacle geometries.³⁹⁻⁴¹ In these models the obstacles are impenetrable for the tracer, and the shape and size distribution of the obstacles are arbitrarily assumed. In reality, lipid molecules may change their state from fluid to gel (or from gel to fluid), and thus the tracer can be part of an obstacle for a shorter or longer period of time. If the tracer can penetrate the obstacles, percolation still occurs but its effects are much smaller. The models for penetrable obstacles⁴²⁻⁴⁵ again assume arbitrarily selected shapes and size distributions for the obstacles.

Lattice models of one- and two-component lipid bilayers have simulated the shape, size, and number of gel/fluid clusters and have predicted equilibrium averages, such as excess heat capacity vs temperature, in agreement with experimental data. The model of Pink⁴⁶ for one-component lipid bilayer is formulated in terms of ten conformational states of each hydrocarbon chain, of which one is the fully ordered all-trans conformation and one is a highly excited liquid crystalline state. The eight remaining states are intermediate chain states, which may be viewed as low-energy excitations of the all-trans state. These eight states and the all-trans state are characteristic of the gel phase. A triangular lattice is used to position the hydrocarbon chains. The Pink model has been extended to assess equilibrium and nonequilibrium lateral distribution of gel/fluid state molecules in nonideal binary lipid mixtures.⁴⁷⁻⁵⁰

Recently we developed a simpler, two-state lattice model of one- and two-component bilayers.^{51,52} Each acyl chain exists in either gel or fluid state with either low or high degeneracy, respectively. Similar to Pink's model, the acyl chains are located at the lattice points of a triangular lattice, but a phospholipid molecule is represented by a pair of nearest neighbor acyl chains, linked covalently to each other. This representation of a phospholipid molecule is needed in binary system to properly calculate the mixing entropy of the components and the percolation threshold concentration of the compositional clusters.^{52,53} By using Monte Carlo methods the two-state model properly simulates the lateral distribution of the components and gel/fluid acyl chains in DMPC/DSPC bilayer. A more detailed description of the model and the respective Monte Carlo methods can be found in the Methods section. The model successfully predicts the excess heat capacity curves,⁵⁴ FRAP threshold temperatures,⁵² and percolation threshold temperatures of compositional clusters⁵³ at different mole fractions and estimates the most frequent center-to-center distance between DSPC clusters at different temperatures, the fractal dimensions of gel clusters,⁵⁵ and the upper bound for the size of small, nonpercolated gel clusters.⁵⁶ By analyzing the simulated lateral distributions we are able to characterize the average geometrical properties of the gel and fluid clusters, such as cluster perimeter, cluster size, number of arms along the cluster perimeter, and number and size of inner islands in a host cluster.⁵⁵

Our goal in this paper is to use a relatively simple, but physically reasonable model using experimental results to describe equilibrium lateral diffusion in binary lipid bilayers leading to our further understanding of existing experimental results and generate experimentally testable predictions. We apply the two-state model to simulate the lateral diffusion of intrinsic molecules in an equimolar DMPC/DSPC bilayer. In the Methods section an abbreviated description of the model and the utilized Monte Carlo methods is presented, while a detailed description is given about the estimation of the time of a diffusion step. In the Results and Discussion section simulated average first-passage time curves are analyzed. Membrane heterogeneity and the properties of the components' lateral diffusion are found to be highly correlated. The relative diffusion coefficient of DMPC calculated from our simulations and as measured by two-dimensional NMR spectroscopy are compared.

Methods

Model of DMPC/DSPC Bilayers. A two-state Ising-type model of DMPC/DSPC lipid bilayers^{52,54} is utilized to simulate the lateral movement of lipid components in both homogeneous and heterogeneous membrane structures. In this section only a brief description of the model is given. Assuming symmetry of the lipid bilayer, only a single monolayer is modeled as a triangular lattice of N points. All acyl chains of DMPC (component 1) and DSPC (component 2) in either gel (state 1) or fluid (state 2) state are located at the lattice points of the triangular lattice. It was experimentally shown that the chains of the lipid molecules in the gel state are organized on a triangular lattice.^{57,58} At the gel-to-fluid transition, the crystalline order is lost and lipid chains become fluid disordered, but the chains remain closely packed. The best lattice to model the position of these closely packed double-chain molecules is again the triangular lattice.

In our model a phospholipid molecule is represented by a pair of nearest neighbor acyl chains, linked covalently to each other. The number of DMPC and DSPC molecules is $N/2$ and

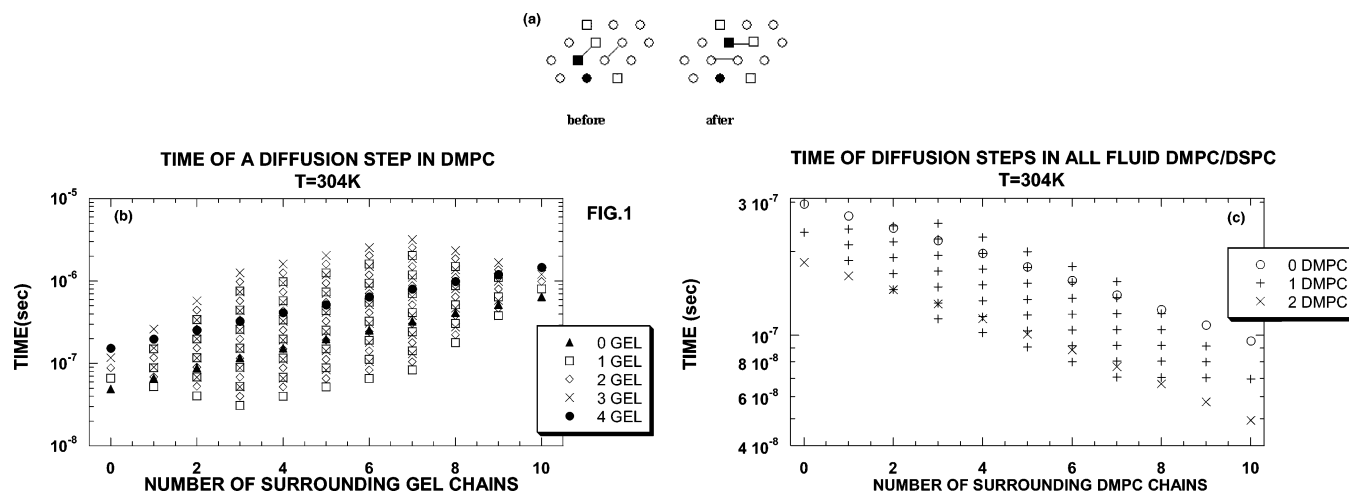


Figure 1. Schematic of local configurations before and after a diffusion step. During the diffusion step the two moving molecule partially exchange positions. Each lattice point represents a hydrocarbon chain. Chains connected by a solid line form a lipid molecule. DMPC chain in gel state is black square, DSPC chain in gel state is black circle, DMPC chain in fluid state is open square, DSPC chain in fluid state is open circle. (b) Calculated time of a diffusion step at different local configurations in a one-component DMPC bilayer. The local configurations are characterized by (1) the number of gel state chains from the 10 chains surrounding the two moving molecules (see horizontal axis), and (2) the number of gel state chains from the 4 chains of the moving molecules. The time of the diffusion step is marked by closed triangle, square, diamond, slanting cross and closed circle in the case of 0, 1, 2, 3, and 4 gel state chains, respectively. Every calculation was performed at 304 K, by using eqs 1–6, 9–11, and the parameter values in Table 2. (c) Calculated time of a diffusion step at different local configurations in an all-fluid two-component DMPC/DSPC bilayer. The local configurations are characterized by (1) the number of DMPC chains from the 10 chains surrounding the two moving molecules (see horizontal axis), and (2) the number of DMPC molecules from the two moving molecules. The time of the diffusion step is marked by open circle, cross and slanting cross in the case of 0, 1, and 2 DMPC molecules, respectively. Every calculation was performed at 304 K, by using eqs 1–6, 9–11, and the parameter values in Table 2.

$N_2/2$, respectively, where $N_1 + N_2 = N$ is the total number of the lattice points. Every lattice configuration can be uniquely described by a square matrix S and a connection vector c , both composed of N elements. Each one of the S matrix elements can take values 1, 2, 3, or 4, corresponding to the DMPC acyl chain in the gel state, the DSPC acyl chain in the gel state, the DMPC acyl chain in the fluid state, and the DSPC acyl chain in the fluid state, respectively. The i th element of the connection vector c_i defines the location of the acyl chain covalently attached to the acyl chain at the i th lattice point. This representation of a phospholipid molecule is needed in binary systems to properly calculate the mixing entropy of the components and the percolation threshold concentration of the compositional clusters.^{52,53}

The energy function of the system is the sum of intrachain and interchain energy terms. The intrachain energy E_j^m of an acyl chain of component j in state m is assumed constant and independent of location and orientation of the rotational isomers. The number of possible locations and orientations of the rotational isomers is characterized by f_j^m , the degeneracy of the energy level of component j in state m . E_{jk}^{mn} is the interchain energy between component j in state m and component k in state n . Only nearest neighbor interactions are considered between the acyl chains since they are short-range van der Waals interactions. When calculating lattice energy, periodic boundary conditions are applied in order to eliminate the effects of the lattice edges⁵⁹ and also to reduce the number of model parameters.⁵⁴ When fitting the model to calorimetric data, the strategy of consecutive parameter estimation was utilized to obtain a robust set of model parameters (see the Determination of Model Parameters section and Table 1 in ref 52). The analysis of the bilayer energy distribution function revealed that the gel–fluid transition is a continuous transition through equilibrium states for DMPC, DSPC, and DMPC/DSPC mixtures; i.e., the system is above a critical point.

Steps in the Monte Carlo Simulations. In our two-state model, the bilayer is only in thermal contact with its surrounding

(canonical ensemble). The thermal fluctuations of DMPC/DSPC bilayers are simulated by means of Monte Carlo methods. The steps of the simulation have been described in detail elsewhere.^{52,54} Each simulation starts from an either all-gel or all-fluid state with similarly oriented molecules. During the equilibration, trial configurations are generated in three different elementary steps: (Step 1) by changing the state of a randomly selected acyl chain from gel to fluid or from fluid to gel, (Step 2) by exchanging two randomly selected molecules of different lipid components, (Step 3) by changing the orientation of a pair of randomly selected nearest neighbor molecules. If the position of the four acyl chains of the selected molecules define the nodes of a rhombus then the orientation of the molecules is changed as it is shown in Figure 1a. Note that by changing the orientation of a pair of molecules both the orientation and the position of the individual molecules are changed. Thus Step 3 is simultaneously a rotational and translational diffusion step. Each trial configuration is accepted or rejected according to the Metropolis criterion.⁶⁰ A series of such elementary steps drives the system to equilibrium, i.e., to the equilibrium distribution of the molecules. The chain of elementary steps can be divided into Monte Carlo cycles. During each Monte Carlo cycle, the system has the opportunity to realize all of its configurations at least once. In our simulations, each Monte Carlo cycle consists of $2N$ elementary steps of local state alterations, followed by N_1 (or N_2 if $N_2 > N_1$) exchange steps and $4N/3$ reorientation steps. At the end of each Monte Carlo cycle, the state of each acyl chain is altered from gel to fluid or from fluid to gel. This nonphysical trial state generation is used to accelerate the attainment of the equilibrium distribution.⁶¹

In this paper the conditions of each simulation are (1) lattice size = 40×40 , (2) number of Monte Carlo cycles = 1 million, with two trials of state change and 2000 trials of local diffusion in each cycle (see next section), and (3) number of equilibration cycles = 5000, with 3200 trials of state change and 2000 trials of local diffusion in each cycle. This lattice size is sufficiently large to model the gel-to-fluid transition of DMPC/DSPC

mixtures from 0.2 to 0.9 DSPC mole fractions.⁵² Simulations on a 100×100 lattice resulted in similar excess heat capacity curves.⁶²

Simulation of Single Particle Tracking. After the attainment of equilibrium, only physically correct elementary steps will be made to simulate the lateral diffusion of lipid molecules: (Step 1) for local state change and (Step 3) for local diffusion. By skipping (Step 2), a nonphysical step, we get continuous tracks of the particles. The relative frequency of state change f_s vs diffusion step f_d is not a priori known. Hac et al.^{62,63} measured the diffusion constant in an equimolar DMPC/DSPC supported multilamellar planar membrane by means of fluorescence correlation spectroscopy (FCS). They used our two-state DMPC/DSPC model to analyze their FCS data. The model simulated correctly the correlation function of the fluctuation of the fluorescence intensity when the frequency of the diffusion step was assumed to be 1000 times greater than the frequency of the state change, and this frequency ratio is used in this work as well. We note that the f_s/f_d frequency ratio has a profound effect on the diffusion. When it approaches zero, the molecules tend to remain in the same state during the diffusion process. In this case a molecule situated initially in a fluid state region tends to travel in a fluid region and completes a certain distance faster than a molecule that can change state and become part of a gel state cluster. This does not mean, however, that a fluid state molecule is unable to cross large gel clusters. The chains remain in the same state when $f_s/f_d = 0$. In this case we ran simulations below the percolation threshold temperature of the gel clusters and it was found that the tracked fluid state molecules were able to penetrate through the large percolated gel cluster.

In our simulations a randomly picked molecule is tracked until its radial distance from the initial position becomes greater than half of the lattice size, i.e.: $\sqrt{3}N/4$ in lattice units. The molecule's location, state, and immediate surrounding is determined at every successful diffusion step and stored for further statistical analysis. For more efficient data collection one can simultaneously track several molecules. Once a tracked molecule reaches the above set limit distance a new molecule can be picked and tracked. The time when a tracked molecule passes for the first time a certain radial distance, r , from its initial position is called first-passage time, $t_{\text{first}}(r)$. One can calculate from the accumulated tracking data the average first-passage time for different radial distances from the initial position of the tracked molecules, $\langle t_{\text{first}}(r) \rangle$. We give a common characterization of the diffusion of intrinsic molecules by the simulated average first-passage time curves.⁶⁴ We note that it is computationally easier to calculate the average first-passage time curve rather than the $\langle r^2 \rangle$ vs time curve. To calculate the average of the square of the distance from the initial position of the molecule one has to consider all the possible paths of the molecule traveled in a given time. In this case the longest of these paths defines the size of the lattice needed for a correct simulation. However, to calculate the average first-passage time of the molecule one need only consider all the possible paths of the molecule within a finite circle around the initial position of the molecule. In this case the diameter of the circle defines the size of the lattice needed for correct simulation. Since the diameter of the circle is much smaller than the length of the paths within the circle, the correct calculation of the average first passage time is computationally much less intensive.

Estimating the Time of a Diffusion Step in One-Component One-State Bilayer. The time when a tracked molecule passes for the first time a certain radial distance from

its initial position is called first-passage time. To calculate the first-passage time one has to estimate the time of each step during the diffusion of the tracked molecule, and then the sum of the time of each diffusion step along the considered path gives the first passage time. Saxton¹³ estimates the time of a diffusion step in fluid phase as follows: for a lipid spacing of 0.8 nm and a diffusion coefficient of $D = 5 \mu\text{m}^2/\text{s}$, the equation $\langle r^2 \rangle = 4Dt$ implies that the time to diffuse one lattice constant is $t = 32$ ns. This estimation is valid for a one component fluid bilayer at a given temperature, e.g., DPPC bilayer at 320 K (see Table 1). In the case of a two-component bilayer existing in the mixed phase region the time of a diffusion step depends on the actual state and type of the diffusing molecule and its immediate surrounding. In this more complex case the estimation will be made by using a generalized version of the free volume theory.

The free volume theory originally has been developed for molecular transport in dense fluids.⁶⁶ This theory was proved to be applicable for lateral diffusion of intrinsic molecules in one-component, one-state lipid bilayers.^{16,67} The theory assumes that the actual number of jumps taken by the molecule per unit time (i.e., the transition frequency) equals the speed with which the molecule can move into an adjacent site, u_{jump} , times the probability that the space into which the molecule is moving is sufficiently large to allow the jump, p_{jump} . Note that in a one-component, one-state bilayer the energy is the same before and after the jump, and thus the energy difference does not affect the transition frequency. When calculating the jump velocity it is assumed⁶⁸ that the bilayer is sufficiently dense and the molecule is confined to the site over a period of time sufficiently long that it undergoes many collisions with its neighbors. The consequence of this Markovian assumption is that the molecule loses its sense of direction and, at thermal equilibrium, its center of mass will have an average velocity $u_{\text{jump}} = \sqrt{2kT/m}$ where m is the mass of the molecule, T is the absolute temperature, and $k = 1.38 \times 10^{-16}$ erg/°C. The free volume per molecule is assumed to follow a Poisson distribution,⁶⁶ and thus the probability that the free volume is larger than b , the minimal space needed for the jump, is $p_{\text{jump}} = \int_b^\infty (1/\langle v_{\text{free}} \rangle) \exp(-v/\langle v_{\text{free}} \rangle) dv_f = \exp[-b/\langle v_{\text{free}} \rangle]$, where v_f and $\langle v_{\text{free}} \rangle$ is the actual and average free volume around the diffusing molecule, respectively. Thus, according to the free volume theory for a one-component one-state system the diffusion coefficient for square lattices is

$$D_{\text{loc}} = \frac{1}{4} \lambda u_{\text{jump}} p_{\text{jump}} = \frac{1}{4} \lambda \sqrt{\frac{2kT}{m}} \exp\left(-\frac{b}{v-a}\right) \quad (1)$$

while the average jump time, t_{jump} , and transition frequency, k_{jump} , of a diffusion step is

$$t_{\text{jump}} = \frac{\lambda}{u_{\text{jump}} p_{\text{jump}}} = \lambda^2 / (4D_{\text{loc}})$$

and

$$k_{\text{jump}} = \frac{1}{t_{\text{jump}}} = \frac{1}{\lambda} \sqrt{\frac{2kT}{m}} \exp\left(-\frac{b}{v-a}\right) \quad (2)$$

where $v - a = \langle v_{\text{free}} \rangle$, a is the close-packed volume of the diffusing molecule, v and m are specific volume and mass of the diffusing molecule, λ is the lipid spacing, and $b (= \gamma_0 a)$ is the minimal free volume needed for the jump where $0.5 < \gamma_0 < 1$. In eq 1 the factor 1/4 signifies that in the case of a square lattice the particle can jump in four directions with the same

TABLE 2: Estimated Values of Model Parameters a and b of Eq 1

| | a ($\text{\AA}^3/\text{molecule}$) | b ($\text{\AA}^3/\text{molecule}$) | temperature interval of fitting (K) |
|--------------|---|---|--|
| DMPC (gel) | 1001.6 ± 0.72 | 759.9 ± 8.5 | 273–305 |
| DSPC (gel) | 1168.0 ± 0.83 | 1101.7 ± 10.9 | 290–305 |
| DMPC (fluid) | 1053.7 ± 0.71 | 434.7 ± 4.9 | 290–330 |
| DSPC (fluid) | 1251.7 ± 0.77 | 669.2 ± 6.1 | 300–340 |

jump probability. However, in calculating the jump time, from eq 2, the lattice geometry does not play a role. One can determine the values of the model parameters a and b for one-component DMPC and DSPC bilayers in an all fluid or all gel phase by fitting eq 1 to the observed temperature dependences of the diffusion constants (see Table 1). Note that we keep the 1/4 factor in the case of our one-component DMPC (or DSPC) model. This assumes that each diffusing molecule has four equally probable ways to jump. In our bilayer model during the diffusion step, two parallel-oriented nearest neighbor molecules rotate by $\pm 60^\circ$ (see Figure 1a). That is two possibilities. Assuming that each diffusing molecule has, on the average, two parallel-oriented nearest neighbor molecules that can rotate, which adds two equally probable possibilities. In eq 1 the following temperature dependencies of the specific volume, in $\text{\AA}^3/\text{chain}$ units, were determined using densitometry data of Nagle and Wilkinson:⁶⁹

$$v_{\text{DMPC}}^g = 390.0026 + 0.46885T \quad (3)$$

$$v_{\text{DSPC}}^g = 457.331 + 0.553T \quad (4)$$

$$v_{\text{DMPC}}^f = 464.259 + 0.28922T \quad (5)$$

$$v_{\text{DSPC}}^f = 555.8835 + 0.33707T \quad (6)$$

The estimated parameter values, a and b , are listed in Table 2. Note that, except for DMPC(fluid), $0.5 < \gamma_o (=b/a) < 1$, and for every fit the correlation parameter r is greater than 0.999. The mass of a mole DMPC and DSPC molecule is 678 and 790 g, respectively.

Note that the temperature dependence of D_{loc} in the free volume theory (eq 1) is not a simple exponential function. Diffusion measurements in a narrow temperature range, however, are unable to reveal the deviation from a simple exponential temperature dependence and usually a simple exponential function is fitted to the data.³⁵ Vaz et al.⁶⁷ by measuring the diffusion in a broader temperature range were able to demonstrate that the temperature dependence is in agreement with the prediction of the free volume theory.

Estimating the Time of a Diffusion Step in a Two-Component Two-State Bilayer. In the case of a two-component bilayer existing in the mixed phase region, the time of a diffusion step depends on the actual state and type of the diffusing molecule and its immediate surrounding. In this more complex case the time estimation is made by generalizing the free volume theory of lipid diffusion for heterogeneous systems. Every process in a lattice model can be described by the following discrete configuration and continuous time master equations:

$$\frac{dP_i}{dt} = \sum_{\{j\} \rightarrow i} k_{j \rightarrow i} P_j(t) - \sum_{i \rightarrow \{j\}} k_{i \rightarrow j} P_i(t) \quad (7)$$

for every i configuration, where $P_i(t)$ is the probability that the system is in the i th configuration at time interval $(t, t+dt)$, and

$k_{i \rightarrow j}$ is the transition frequency from configuration i to j . In the case of equilibrium, the left-hand side of the master equations is zero and at any time the probability over the configurations follows a Boltzmann distribution

$$P_i(t) = P_i^{\text{eq}} = e^{-E_i/kT} / \sum_{\{h\}} e^{-E_h/kT} \quad (8)$$

where E_i is the system's energy in the i th configuration. In quantum mechanics, the calculation of the transition frequencies is strictly defined, but in classical theories their form is only partially constrained by the principle of detailed balance. In our calculations the following definition of the transition frequencies, satisfying the principle of detailed balance, is utilized (see Appendix 1):

$$k_{i \rightarrow j} = v_{ij}(T) e^{(E_i - E_j)/2kT} \quad (9)$$

where the preexponential factor may depend on temperature and should depend symmetrically from the initial and final configuration of the transition, i.e., $v_{ij} = v_{ji}$.

In the case of a one-component, one-state bilayer, the energy of the initial and final configuration of a diffusion step is the same, and thus $k_{i \rightarrow j} = v_{ij}(T)$, where $v_{ij}(T)$ can be obtained from the free-volume theory (i.e., $k_{\text{jump}} = v_{ij}(T)$, see eq 2).

For a two-component, two-state system, however, the energy of the initial and final configuration of a diffusion step can be different and we have to use eq 9 to calculate the transition frequency. This energy difference, $E_i - E_j$, is originated only from the change in the interchain interactions, because during a diffusion step the state of the diffusing molecule does not change. The preexponential factor in eq 9 can be calculated by means of a free-volume theory generalized for heterogeneous systems. Because of the heterogeneity of the system the average local free volume, $\langle v_{\text{free}} \rangle$, and the local minimum free volume, b needed for the jump depends on the local configuration around the diffusing molecule. One can define the average local free volume per chain by

$$\langle v_{\text{free}} \rangle = \frac{1}{14} \sum_{i=1}^{14} [v_i(T) - a_i] \quad (10)$$

and the local minimum free volume per chain by

$$b = \frac{1}{14} \sum_{i=1}^{14} b_i \quad (11)$$

where the summation is taken for the four chains involved in the diffusion step and their 10 nearest neighbor chains. The value of v_i , a_i , and b_i depends on the type and state of the i th chain and listed in eqs 3–6 and Table 2.

To obtain the same time for the diffusion step of both molecules, the average mass, $m = (m_1 + m_2)/2$ of the moving molecules is inserted into eq 1. Figure 1b and c show the average time of a diffusion step, t_{jump} , calculated by using eqs 1–11 at different local configurations of a 14-chain unit shown in Figure 1a. The calculated time is different for different local configurations, but we can observe the following trends. (1) The time of a diffusion step is broadly distributed. At 304 K the time of a diffusion step is distributed from 3×10^{-8} to 3×10^{-6} s for one-component DMPC membrane, and from 5×10^{-8} to 3×10^{-7} s for all fluid DMPC/DSPC mixture. (2) If the 4-chain moving unit has a homogeneous surrounding, the time of diffusion step decreases with increasing number of DMPC and/or fluid-state chains in the 4-chain moving unit. (3) However,

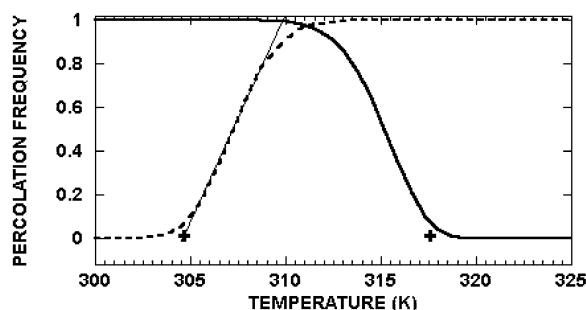


Figure 2. Calculated percolation frequency curves of gel (solid line) and fluid (dashed line) clusters of equimolar DMPC/DSPC bilayers. The percolation threshold temperature of gel and fluid clusters is marked by a cross at 317.5 and 304.6 K, respectively. A straight line is fitted to the inflection point of the percolation frequency curve and its intercept with the zero frequency line defines the percolation threshold temperature. (This figure is adapted from ref 55.)

if the 4-chain moving unit has a heterogeneous surrounding, the energy difference between the initial and final configuration will primarily determine the time of the diffusion step.

Results and Discussion

Cluster Percolation and Long-Range Diffusion. In fluorescence recovery after photobleaching (FRAP) experiments, the diffusion of probe molecules is measured. The probes may disturb the local membrane structure and exist preferentially in fluid phase regions. The long-range diffusion of the probe is blocked below the FRAP threshold temperature. Our two-state DMPC/DSPC model shows a strong correlation between the FRAP threshold temperatures and the percolation threshold temperatures of gel clusters. A snapshot of the simulated equilibrium configurations is percolated if a cluster, probably the largest one, spans the lattice either horizontally or vertically. The ratio of the number of percolated snapshots to the number of all analyzed snapshots is the percolation frequency. In Figure 2 the calculated temperature dependence of the percolation frequency is shown for both gel and fluid clusters in an equimolar mixture of DMPC/DSPC. A straight line fitted to the inflection point of the percolation frequency curve and its intercept with the zero frequency line defines the percolation threshold temperature: 304.6 K and 317.5 K for fluid and gel clusters, respectively (see crosses in Figure 2).

Vaz and co-workers²¹ assumed that the FRAP threshold temperature is related to the percolation threshold temperature. They assumed the same percolation threshold temperature for gel and fluid clusters, i.e., at the temperature where small gel clusters become connected forming a very large cluster, simultaneously the very large fluid cluster becomes disconnected into many small fluid clusters. However, it was pointed out recently that the two percolation threshold temperatures are different for every mixing ratio, except in the case of ideal mixtures.⁵³ For the rather nonideal DMPC/DSPC mixture the percolation threshold temperature of gel clusters is significantly higher than for fluid clusters at every mixing ratio, except for pure DMPC or pure DSPC (Figure 2 and 3). Our simulations show strong, positive correlation, with a constant difference of +1.8 °C, between the calculated percolation threshold temperatures of gel clusters and the FRAP threshold temperatures (closed circles in Figure 3) measured by Vaz et al.²¹ However, the measured FRAP threshold temperatures are in complete agreement with the temperatures where the percolation frequency of the gel clusters is 0.36 (closed squares in Figure 3). It is important to note that the correlation of the FRAP threshold

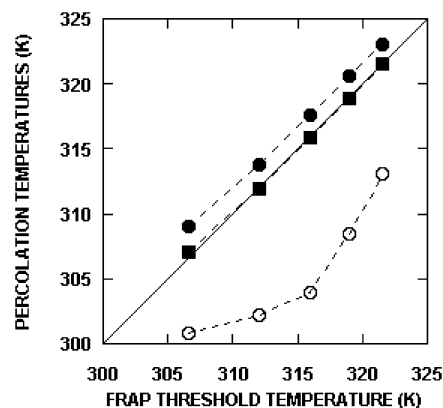


Figure 3. Calculated percolation threshold temperatures versus FRAP threshold temperatures measured at different DMPC/DSPC mole fractions (Vaz et al., 1989). Closed circles: percolation threshold temperatures of gel clusters; open circles: percolation threshold temperatures of fluid clusters; closed squares: temperatures at 0.36 percolation frequency of gel clusters. (This figure is adapted from ref 55.)

temperatures with the percolation threshold temperatures of the fluid clusters is weak (open circles in Figure 3). This shows that in the timeframe of the FRAP experiments the largest gel cluster efficiently blocks the fast, long-range diffusion of the probe molecules, which preferentially exist in the fluid regions, if the percolation frequency of the gel clusters is >0.36 .

First-Passage Time Curves. FRAP probe molecules partition exclusively into the fluid phase.²¹ An intrinsic molecule in a DMPC/DSPC mixture, however, may enter from fluid to gel cluster or from gel to fluid cluster. This qualitative difference between FRAP probes and the intrinsic molecules may also result in distinctly different diffusion properties. By using our model we investigate the diffusion properties of the intrinsic molecules in an equimolar DMPC/DSPC mixture by estimating the first-passage time, t_{first} (see Appendix in ref 64). The first-passage time is the time needed for the molecule to reach for the first time a prescribed radial distance from its original position.

In Figure 4 the average first-passage times of DMPC and DSPC molecules, diffusing in an equimolar mixture of DMPC/DSPC, are plotted against the radial distance from the initial position. The average first-passage time curve $\langle t_{\text{first}}^g \rangle$, $\langle t_{\text{first}}^f \rangle$, or $\langle t_{\text{first}}^m \rangle$ is marked by circle, square, or diamond when the molecule is located initially inside a gel cluster, fluid cluster, or gel/fluid interface, respectively. In our definition, the tracked molecule is initially inside a gel (or fluid) cluster if the chains of the two molecules participating in the diffusion step and their 10 nearest neighbor chains are all in gel (or fluid) state, respectively; otherwise, the molecule is at the gel/fluid interface. What is the rationale behind this definition? Geometrically a lipid molecule is defined to be inside a fluid cluster if all its eight nearest neighbor hydrocarbon chains are in the fluid state. In the above definition, however, we require that not only the tracked molecule but also the molecule participating in the diffusion step be initially inside a fluid cluster. This way the molecule initially diffuses similarly to a molecule located in an all-fluid bilayer. This is because the average time of the diffusion step depends on the state of the simultaneously moving pair of molecules and their 10 nearest neighbor chains.

If we do not specify the initial local state of the diffusing component the average first-passage time curve, t_{first} is calculated from $\langle t_{\text{first}}^g \rangle$, $\langle t_{\text{first}}^f \rangle$, and $\langle t_{\text{first}}^m \rangle$ as follows:

$$\bar{t}_{\text{first}} = [h^g \langle t_{\text{first}}^g \rangle + h^f \langle t_{\text{first}}^f \rangle + h^m \langle t_{\text{first}}^m \rangle] / [h^g + h^f + h^m] \quad (12)$$

where h^g , h^f , and h^m is the number of tracked molecules initially situated in gel cluster, fluid cluster, and gel/fluid interface, respectively.

At a given distance, the first-passage time is longest when the molecule starts diffusing from a gel cluster, and shortest when it is initially inside a fluid cluster. At most of the temperatures, the average first-passage time curves are qualitatively similar and can be described by the following power function (exceptions are discussed in a separate section entitled: "Diffusion and Cluster Percolation"):

$$\langle t_{\text{first}} \rangle = \alpha d^\beta \quad (13)$$

where the distance d and the parameter α is given in lattice units (l.u.) and seconds, respectively. α is the average time of diffusing one lattice unit distance, i.e., $d = 1$. In the case of normal diffusion, $\beta = 2$ and α is related to the diffusion coefficient, D as follows:

$$D \propto \frac{\lambda^2}{4\alpha} \quad (14)$$

where λ is the lattice unit given in cm units. This relationship is the result of comparing eq 13 with the equation $\langle \lambda^2 \rangle = 4Dt$ defining the diffusion coefficient for normal diffusion.

The diffusion is considered to be anomalous when $\beta > 2$ or $\beta < 2$, referred to as sub- or super-diffusion,^{13,70,71} respectively, and cannot be described by eq 14. Note that for sub- and super-diffusion at the same α , the average first-passage time of a certain distance is longer and shorter, respectively, than in the case of normal diffusion.

Specified Initial Local State. In cases where the initial local state of the diffusing component is specified, the fitted values of α and β are plotted against the temperature in Figure 5. The correlation coefficient for the fit, r , is greater than 0.999 for every fit. In the fluid-phase region, i.e., above 320 K in equimolar DMPC/DSPC mixture, the diffusion approaches normal behavior (i.e., $\beta = 2$) for each component located initially inside a fluid cluster (see Figure 5a and b). In the gel/fluid mixed phase region (i.e., from 320 K to 300 K in equimolar DMPC/DSPC mixture), components situated initially inside a fluid cluster are involved in sub-diffusion. DSPC molecules situated initially inside a gel cluster or at the gel/fluid interface are also involved in sub-diffusion. However, for DMPC molecules situated initially inside a gel cluster $\beta < 2$ (super-diffusion). For DMPC molecules, situated initially at a gel/fluid interface, the diffusion is close to normal, i.e., $\beta \approx 2$.

Figure 5c and d show the temperature dependence of the α parameter for the diffusion of DMPC and DSPC, respectively. Below, but close to 300 K, and above 320 K, the diffusion is close to normal and the temperature dependence of α can be represented as

$$\alpha \propto \frac{\lambda^2}{4D} = \frac{\lambda^2}{4A} \exp\left(\frac{E_a}{RT}\right) \quad (15)$$

where the diffusion coefficient D is substituted by the Arrhenius equation (see the legend to Table 1) in the second equality, and E_a is the activation energy of the diffusion. In Figure 5c,d the dashed and dotted lines show the temperature dependence of α , calculated by eq 15, for one-component all-gel and all-fluid bilayer, respectively. In the fluid/gel mixed phase region the actual α values deviate significantly from the expected values

for normal diffusion. It is especially anomalous that α increases with increasing temperature for molecules, located initially in a fluid state region. In the case of a DMPC molecule, situated initially in a mixed state region, the diffusion is very close to normal ($\beta \approx 2$) even in the 300–320 K temperature region and one can use Figure 5c and eq 14 to calculate the diffusion coefficient, but the exponential temperature dependence, given by eq 15, does not hold.

Unspecified Initial Local State. In the case of unspecified initial local state of the diffusing component, the average first-passage time curve, \bar{t}_{first} , is calculated from the respective average first-passage time curves of specified initial states $\langle t_{\text{first}}^g \rangle$, $\langle t_{\text{first}}^f \rangle$, and $\langle t_{\text{first}}^m \rangle$ by using eq 12. One can fit eq 13 to this average first-passage time curve, \bar{t}_{first} (not shown). In the case of unspecified initial local states the fit is excellent at any temperature ($1 > r > 0.9999$), but when the initial local state is specified a good fit can be obtained with certain restrictions (see section entitled Diffusion and Cluster Percolation). The fitted values of α and β are plotted against the temperature in Figure 6. In the fluid phase, above 325 K, $\beta \approx 2$ and thus the diffusion of the components is normal. In the gel/fluid mixed phase region, from 320 K to 300 K, $\beta > 2$ for each component, and thus each component is involved in sub-diffusion. In the gel/gel mixed phase region, β for DMPC increases from 2.03 to 2.07 while the temperature decreases from 300 K to 270 K, i.e., the diffusion is increasingly anomalous sub-diffusion.

Lateral Distribution of the Components and the Type of Their Diffusion. It is important to determine the reason for anomalous diffusion of intrinsic molecules in DMPC/DSPC bilayers. It cannot be associated with the gel and fluid state of the components because during the diffusion process a molecule may change its state at any time. In this section we point out that the type of the diffusion, characterized by β , is correlated with the lateral distribution of the components.

Characterizing the Lateral Distribution of the Components. By using the same two-state model of DMPC/DSPC bilayers, Michonova-Alexova and Sugar⁵³ calculated the size distributions of the DMPC and DSPC compositional clusters at different temperatures and mole fractions. After analyzing the cluster size distributions, the percolation threshold concentration of DMPC and DSPC clusters were determined at different temperatures and plotted on the temperature/mole fraction plane. In Figure 7, the heavy solid line at the left and right-hand side show the percolation threshold concentrations of DSPC and DMPC clusters, respectively, at different temperatures. Further analysis of the size distributions of the compositional clusters revealed that the heavy solid lines in Figure 7 enclose a region of the temperature-mole fraction plane where the components are nonrandomly distributed, while outside of this region the distribution is random. In Appendix 2 we give a detailed description of the analyses of the cluster size distributions and the construction of the diagrams in Figure 7. The two vertical dash-dotted lines on the left and right side of the diagram refer to the percolation threshold concentrations of the randomly distributed DSPC and DMPC molecules, respectively, at different temperatures. At temperature T , $\Delta_{\text{DMPC}}(T)$ and $\Delta_{\text{DSPC}}(T)$ is the horizontal distance between the heavy solid line and the respective dash-dotted line (see double arrows in Figure 7). In an equimolar DMPC/DSPC mixture, we can characterize the deviation of each component from a random lateral distribution using $\Delta_{\text{DMPC}}(T)$ and $\Delta_{\text{DSPC}}(T)$. For example, from 330 K the heavy solid lines coincide with the respective dash-dotted lines, i.e., in accordance with the small-angle neutron scattering data, the distribution of the components is random.^{53,72,73}

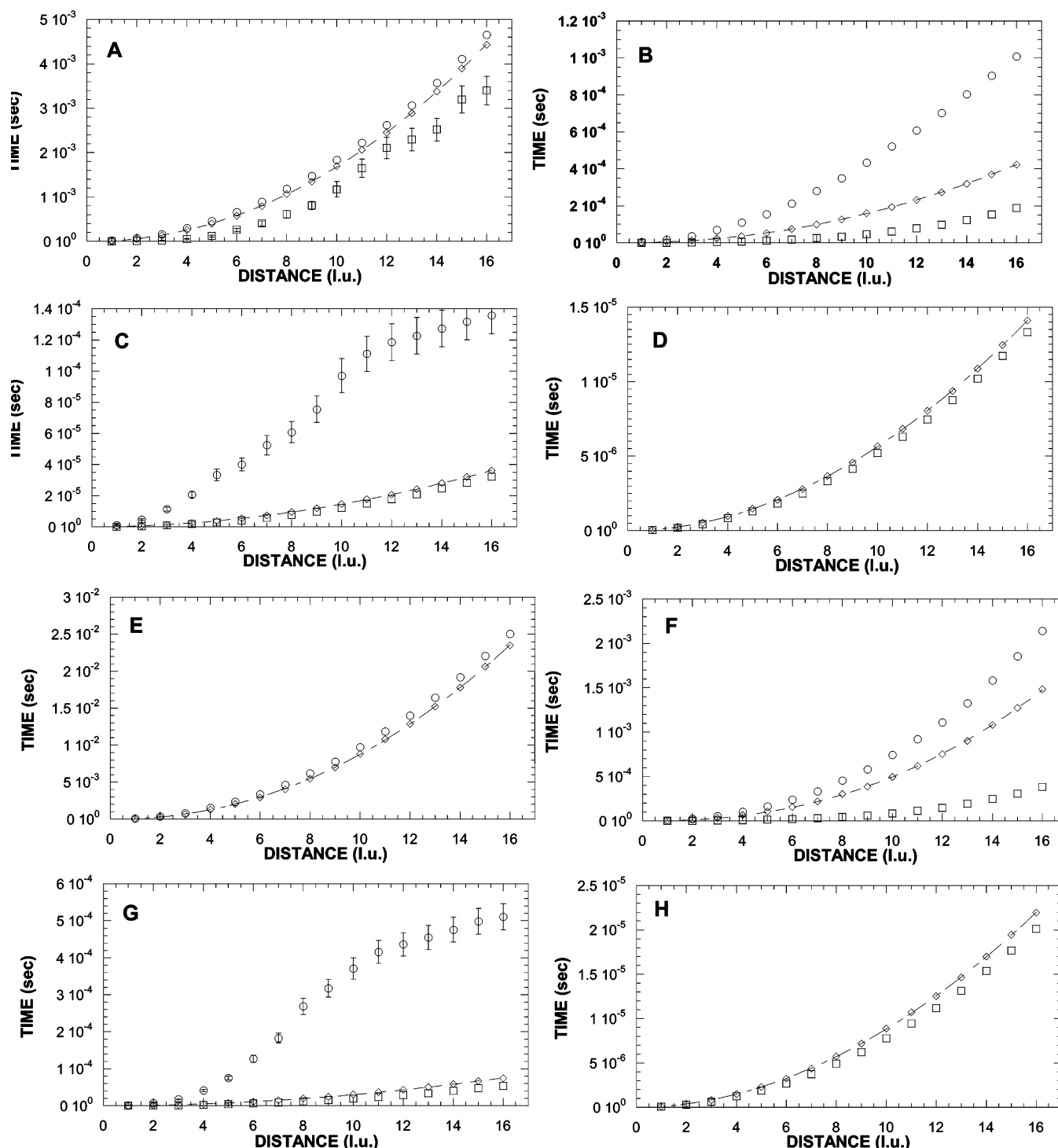


Figure 4. Calculated average first-passage time curves with specified initial local state in equimolar DMPC/DSPC bilayer. Figure (a), (b), (c), and (d) plot the average first-passage time of DMPC against its traveled radial distance at 300 K, 310 K, 320 K, and 330 K, respectively. Figure (e), (f), (g), and (h) plot the average first-passage time of DSPC against its traveled radial distance at 295 K, 310 K, 320 K, and 330 K, respectively. The distance is measured in lattice units (l.u.), while the first passage time is measured in seconds. The average first-passage time curve $\langle t_{\text{first}}^g \rangle$, $\langle t_{\text{first}}^f \rangle$, or $\langle t_{\text{first}}^i \rangle$ is marked by circles, squares, or diamonds when the tracked molecule is initially inside a gel cluster, fluid cluster, or at the gel/fluid interface, respectively. In our definition the tracked molecule is initially inside a gel (or fluid) cluster if the chains of the two molecules participating in the diffusion step and their 10 nearest neighbor chains (see Figure 1a) are all in gel (or fluid) state, respectively, otherwise the molecule is at the gel/fluid interface (see text for the rationale of this definition).

In Figure 7 there are also two dashed lines, representing the calculated phase diagram of the DMPC/DSPC bilayers. The calculated phase diagram is in agreement with the phase diagram constructed by using the measured excess heat capacity curves.⁵² The dashed lines at lower and higher temperatures are the solidus and liquidus lines, respectively. Above the liquidus line is the region of the fluid phase, where the components are in fluid

state and randomly distributed. In the gel/fluid mixed phase region, situated between the solidus and liquidus lines, fluid and gel-state clusters coexist and the components are nonrandomly distributed. In the gel/gel mixed phase region, situated below the solidus line and between the heavy solid lines, the components are in gel state and nonrandomly distributed. Out of the region of the heavy solid lines, however, the components

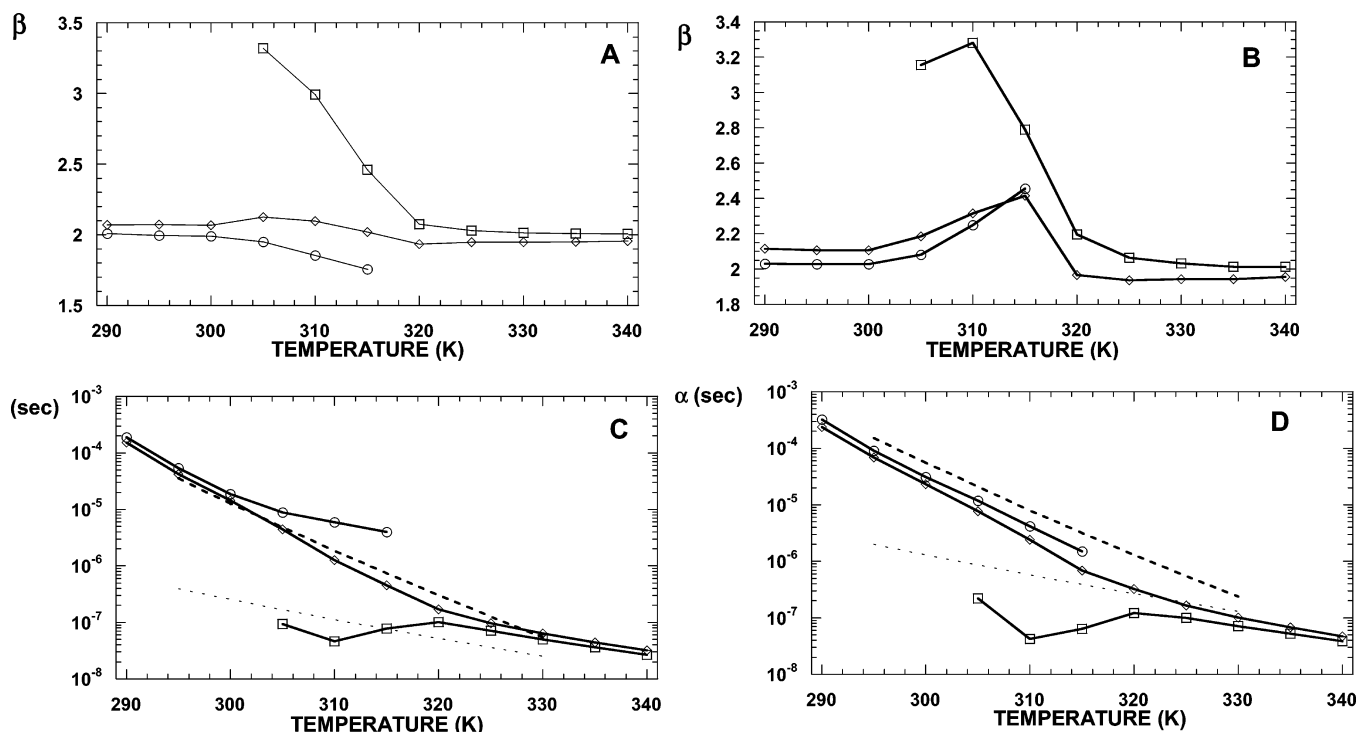


Figure 5. Parameters of the diffusion of the intrinsic molecules with specified initial local state in equimolar DMPC/DSPC bilayers. The parameters α and β of eq 13 are estimated by fitting the equation to the simulated average first-passage time curves $\langle t_{\text{first}}^g \rangle$, $\langle t_{\text{first}}^f \rangle$, and $\langle t_{\text{first}}^m \rangle$. The estimated β parameter for DMPC and DSPC is plotted against the temperature in panels (a) and (b), respectively. The estimated α parameter for DMPC and DSPC is plotted against the temperature in panels (c) and (d), respectively. Circles, squares, or diamonds mark the curves when the tracked molecule is initially inside a gel cluster, inside a fluid cluster, or at the gel/fluid interface, respectively. In our definition, the tracked molecule is initially inside a gel (or fluid) cluster if the chains of the two molecules participating in the diffusion step and their 10 nearest neighbor chains are all in gel (or fluid) state, respectively; otherwise, the molecule is at the gel/fluid interface. For nonlinear curve fitting a commercially available software (Kaleidagraph 3.09) was utilized. By using this program the value and standard deviation of each model parameter in eq 13 was estimated. The standard deviations of the model parameters (not shown) are smaller than the symbols. Dashed and dotted lines show the temperature dependence of α (calculated by eq 15 and by using the data in Table 1) for one-component all-gel and all-fluid bilayer, respectively.

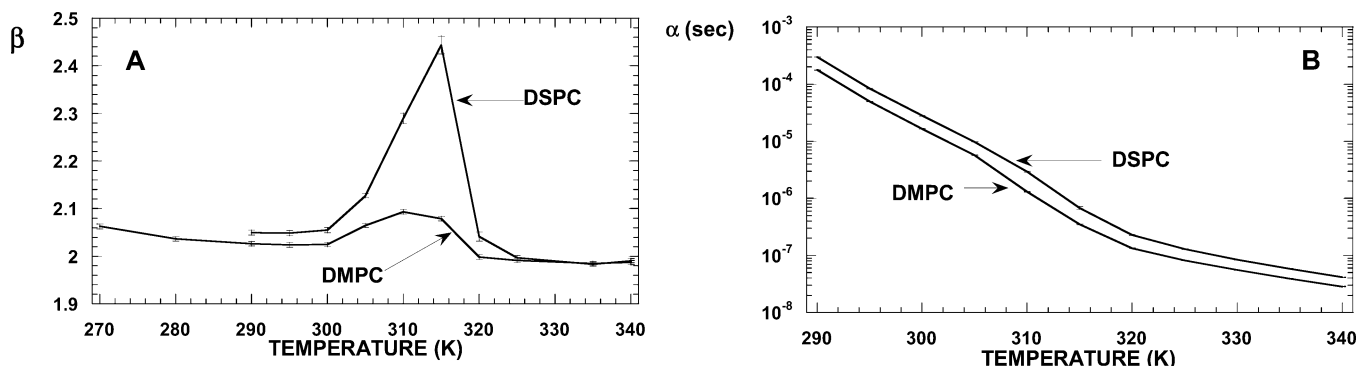


Figure 6. Parameters of the diffusion of the intrinsic molecules with unspecified initial local state in equimolar DMPC/DSPC bilayers. The parameters of eq 13 are estimated by fitting the equation to the average first-passage time curve, t_{first} . The estimated β and α parameter for each component is plotted against the temperature in panels (a) and (b), respectively. The average first-passage time curve, t_{first} has been calculated by using eq 12 and the simulated average first-passage time curves $\langle t_{\text{first}}^g \rangle$, $\langle t_{\text{first}}^f \rangle$, and $\langle t_{\text{first}}^m \rangle$. For nonlinear curve fitting a commercially available software (Kaleidagraph 3.09) was utilized. By using this program the value and standard deviation of each model parameter in eq 13 was estimated (see error bars).

are in gel state and randomly distributed. The calculated distributions of the components in different regions of the phase diagram have been confirmed by small-angle neutron scattering data.^{72,73}

Correlation between β and the Lateral Distribution of the Components. The results of our current simulations clearly show a strong correlation between the type of the diffusion and the lateral distribution of the components. When the component is randomly distributed then it is involved in normal diffusion, $\beta \approx 2$. For example in an equimolar mixture of DMPC/DSPC above 330 K, $\Delta_{\text{DSPC}} = \Delta_{\text{DMPC}} = 0$ (Figure 7), i.e., each

component is randomly distributed, while β is very close to 2 for each component regardless of the initial local state (see Figure 5a,b and Figure 6a).

When the component is nonrandomly distributed and its initial local state is not specified it is involved in sub-diffusion, $\beta > 2$. For example, in an equimolar mixture of DMPC/DSPC within the gel/fluid mixed phase region, $\Delta_{\text{DSPC}} > 0$ and $\Delta_{\text{DMPC}} > 0$ (Figure 7), i.e., the lateral distribution of the components is nonrandom, while $2 < \beta < 2.1$ for DMPC and $2 < \beta < 2.44$ for DSPC (Figure 6a). Below the solidus line, at 295 K, in the gel/gel mixed phase region, $\Delta_{\text{DSPC}} = 0.055$ and $\Delta_{\text{DMPC}} = 0.03$

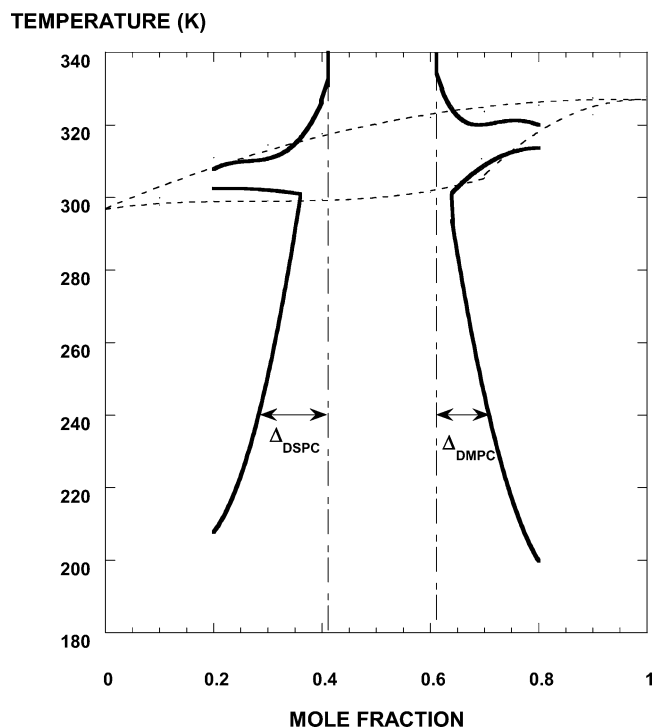


Figure 7. Calculated diagrams of DMPC/DSPC bilayers. Heavy solid lines on the left- and right-hand side give the percolation threshold mole fractions of DSPC and DMPC clusters, respectively, at different temperatures. In the case of randomly distributed components dash-dotted lines on the left- and right-hand side give the percolation threshold mole fractions of DSPC and DMPC clusters. Δ_{DSPC} and Δ_{DMPC} , marked by double arrows, measure the deviation from random distribution for DSPC and DMPC, respectively, in an equimolar DMPC/DSPC mixture at temperature T . The dashed lines at higher and lower temperatures represent the liquidus and solidus lines, respectively, of a calculated DMPC/DSPC phase diagram. The detailed description of the construction of the diagrams is given in Appendix 2. (This figure is adapted from ref 53.)

are close to zero, i.e., the distribution of the components is not random but close to it (Figure 7) and accordingly β is not equal but close to 2 (for DMPC $\beta = 2.04$ and for DSPC $\beta = 2.06$). By decreasing the temperature from 295 K, Δ_{DSPC} and Δ_{DMPC} will increase (Figure 7), i.e., the deviation from a random distribution increases, and accordingly β increases (Figure 6a). It is important to emphasize that in the above cases neither the component's initial state nor its state during diffusion is specified. Sub-diffusion takes place because of the nonrandom distribution of the components and not because the gel clusters obstruct the diffusion of the fluid molecules! As a matter of fact, in the gel phase region where the diffusion of every molecule is "obstructed" by gel state molecules, β is close to 2, e.g., $\beta = 2.01 \pm 0.0067$ for DMPC and $\beta = 1.997 \pm 0.0047$ for DSPC at 305 K and DSPC mole fraction of 0.75.

We tested the correlation between diffusion type and the lateral distribution of components using a multivariate regression analysis.⁷⁴ β characterized diffusion type and $\Delta_{\text{DMPC}}(T)$ and $\Delta_{\text{DSPC}}(T)$ characterized the lateral distribution of components in an equimolar mixture of DMPC/DSPC. We used the following linear model:

$$\beta = a_0 + a_1 \Delta_{\text{DMPC}} + a_2 \Delta_{\text{DSPC}} \quad (16)$$

where a_1 and a_2 are the regression parameters showing the strength of the correlation between β and the lateral distribution of DMPC and DSPC, respectively. When the initial state of the diffusing component is not specified, the estimated values

of a_1 and a_2 are listed in the first two rows of Table 3. The large value of the correlation coefficient, r , listed in the 6th column, shows that the correlation is strong and the model in eq 16 is adequate. In the case of DMPC diffusion, $a_1 \approx a_2$ in an equimolar DMPC/DSPC mixture. Thus the type of DMPC diffusion is correlated equally with the lateral distribution of both components. However, in the case of DSPC diffusion, $a_1 \gg a_2$ in an equimolar DMPC/DSPC mixture. In this case, the type of DSPC diffusion is correlated primarily with the lateral distribution of DMPC molecules.

Using the same multivariate regression analysis, we found a strong correlation between β and the distribution of the components when the initial state of the diffusing component is specified. The results of the analyses for different initial states of the components are shown starting from the third row of Table 3. In all but one case the correlation is positive and the respective diffusion type is sub-diffusion. The correlation is negative in the case of super-diffusion, when DMPC is situated initially in a gel cluster. In this exceptional case β is primarily correlated with the distribution of DMPC (Table 3).

The Physical Cause of the Correlation between β and the Lateral Distribution of Components. In an equimolar mixture of DMPC/DSPC, each component forms one large percolated cluster. The two large clusters contain the majority of molecules forming the bilayer, and thus their structure is of primary importance in the overall diffusional properties of the components.

In the gel/gel mixed phase region at 295 K the distribution of components is nearly random. In this case, the structure of each percolated compositional cluster is very loose, containing many inner islands of the other component. The percolated cluster is so loose that the local concentration of the component is the same everywhere in the bilayer. The average first passage time $\langle t_{\text{first}}(r) \rangle$ of a component depends on the average number of diffusion steps, $\langle n(r) \rangle$, and the average time of a diffusion step, $\langle t_{\text{jump}}(r) \rangle$, until the radial distance of the tracked molecule from its original location becomes r for the first time. When the component is randomly distributed, the average number of diffusion steps is proportional to r^2 (see ref 75). Since the local concentration of the component is the same everywhere, the average jump time is independent from r . Thus we get

$$\langle t_{\text{first}}(r) \rangle = \langle t_{\text{jump}}(r) \rangle \cdot \langle n(r) \rangle \propto r^2, \text{ i.e., } \beta = 2$$

By decreasing the temperature from 295 K, the distribution of the components increasingly deviates from random. The structure of each percolated compositional cluster gets more compact. The number and size of the inner islands of the other component gets smaller. The local concentration of the component increases toward the interior of the percolated compositional cluster (see simulations in gel/fluid mixed phase region in ref 52). For example, DSPC molecules are preferentially located inside the percolated DSPC cluster, and thus a diffusing DSPC molecule, located initially inside the cluster, returns more frequently to its initial location than in the case of randomly distributed components. As the radial distance of the diffusion increases, approaching the edge of the cluster, the DSPC concentration decreases and thus the average number of diffusion steps becomes increasingly larger than in the case of randomly distributed components, i.e. $\langle n(r) \rangle \propto r^{2+\delta}$ where δ is a positive number. Since the DSPC concentration inside the cluster is larger than at the cluster edge, the jump time of the diffusing DSPC molecule inside the cluster is longer than at the edge of the cluster. Thus the average jump time decreases with increasing r , but the decrease should be negligibly small because the

TABLE 3: Estimated Parameters of the Multivariate Regression Model in Eq 16

| tracked component | initial location | a_0 | a_1 | a_2 | r | $a_2/(a_1 + a_2)$ |
|-------------------|---------------------|--------|---------|---------|--------|-------------------|
| DMPC | not specified | 1.9899 | 0.3413 | 0.3348 | 0.905 | 0.495 |
| DSPC | not specified | 1.9652 | 2.0207 | 0.3830 | 0.973 | 0.159 |
| DMPC | gel | 2.0401 | -1.2454 | -0.1730 | -0.980 | 0.122 |
| DMPC | gel/fluid interface | 1.9727 | -0.0034 | 0.7924 | 0.803 | 1.004 |
| DMPC | fluid | 1.9690 | 0.7615 | 5.8010 | 0.982 | 0.884 |
| DSPC | gel | 1.9606 | 2.1879 | 0.1350 | 0.989 | 0.058 |
| DSPC | gel/fluid interface | 1.9485 | 1.8204 | 0.8572 | 0.917 | 0.320 |
| DSPC | fluid | 1.9895 | 2.5879 | 5.0164 | 0.946 | 0.660 |

majority of the jumps take place inside the cluster. Thus we get $\langle t_{\text{first}}(r) \rangle = \langle t_{\text{jump}}(r) \rangle \cdot \langle n(r) \rangle \propto r^{2+\delta}$, i.e., $\beta = 2 + \delta > 2$. One can similarly explain the sub-diffusion of DMPC molecules (located initially inside the percolated DMPC cluster) in the gel/gel mixed phase region.

In the gel/fluid mixed phase region of an equimolar DMPC/DSPC mixture, one percolated gel and one percolated fluid cluster may appear in addition to the two percolated compositional clusters. At the edge of the percolated gel cluster the DMPC concentration is higher than inside the cluster.^{47,48,52} Let us explain the super-diffusion of DMPC molecules, located initially inside this percolated gel cluster. During its diffusion, the DMPC molecule visits regions with higher DMPC concentrations more frequently and reaches a radial distance r with a fewer number of diffusion steps than in the case of randomly distributed components, i.e., $\langle n(r) \rangle \propto r^{2-\gamma}$, where γ is a positive number. Since the molecule spends more time in regions with higher DMPC concentrations, where the jump time of the DMPC molecule is shorter, the average jump time decreases with increasing radial distance, i.e., $\langle t_{\text{jump}}(r) \rangle \propto r^{-\kappa}$, where κ is a positive number. Thus we get $\langle t_{\text{first}}(r) \rangle = \langle t_{\text{jump}}(r) \rangle \cdot \langle n(r) \rangle \propto r^{2-\gamma-\kappa}$, i.e., $\beta = 2 - \gamma - \kappa < 2$.

Effect of Finite Size Scaling. The diffusion of a component was found to be normal when the components of the membrane were randomly distributed, otherwise the diffusion was anomalous. Does this conclusion remain valid when the system size is increased?

We pointed out that the anomalous diffusion of the components is related to the inhomogeneous distribution of the components within the percolated compositional or gel/fluid clusters. The size of the percolated cluster scales with the system size, while the smaller clusters remain small.⁵⁶ Thus in a larger system, if the length scale of the diffusion measurement is comparable with the system size, the diffusion will be similarly affected by the inhomogeneous distribution of the components in the percolated clusters. All of our statements in this paper refer to equilibrium distributions of the components.

In the case of nonequilibrium distribution, the system may contain more than one large, but not percolated, gel or fluid clusters.⁵⁶ If the components are inhomogeneously distributed in these clusters and the length scale of the diffusion measurement is comparable with the size of these large clusters, one can expect anomalous diffusion. However, if the length scale of the diffusion measurement increases, the diffusion approaches a normal diffusion.

The above examples suggest that β strongly correlates with the components' deviation from random distribution. It is important to emphasize that: (1) we obtain normal, super, and sub-diffusion within the framework of the same simple model without assuming specific diffusion mechanisms, and (2) in the case of anomalous diffusion one cannot associate a time independent diffusion coefficient to the process. The possibility of anomalous diffusion in membranes arises because the

diffusing molecule visits a variety of different environments characterized by its relative proximity to various membrane components.^{70,71} However, this is not a sufficient condition for anomalous diffusion, e.g., in the extreme fluid phase region of an equimolar DMPC/DSPC mixture the diffusion is normal. The diffusion is only anomalous when the diffusing molecules are nonrandomly distributed.

Diffusion and Cluster Percolation. In Figure 5 we do not provide α and β values at $T > 315$ K and $T < 305$ K for molecules situated initially in a gel and fluid state region, respectively. Beyond these temperature limits the average first-passage time curves cannot be described by a simple power function. Above 315 K, for molecules situated initially inside a gel cluster, the average first-passage time curves become sigmoidal (see Figure 4c,g) and we cannot fit eq 13 to the simulated data. From 315 K to 320 K the percolation frequency of the gel clusters decreases from 0.5 to 0 (see Figure 2), i.e., there are frequently large but nonpercolated gel clusters. A molecule, initially located in a large gel cluster, diffuses slowly in the gel phase, but eventually reaches the gel/fluid interface changes state and diffuses fast toward the edge of the lattice. The average size of the large gel clusters thus can be characterized by the inflection point of the sigmoidal average first-passage time curve. The size of the large gel clusters, however, strongly fluctuates, because they may coalesce to form a percolated cluster. This cluster size fluctuation is manifested in the increasing fluctuation of the first-passage time beyond the inflection point of the sigmoid. Upon further increasing the temperature, it becomes rare to find a molecule inside a gel cluster, i.e., a cluster of 14 gel chains, and the sample size from our simulations is too small to provide a reliable average first-passage time curve.

Below 305 K, for molecules situated initially inside a fluid cluster, the average first-passage time curve deviates also from a simple power function (eq 13). From 307 K to 304 K there are frequently large fluid clusters, which are rarely percolated (see Figure 2). A molecule, initially located in a large fluid cluster, diffuses fast in the fluid phase, but eventually reaches the fluid/gel interface, changes state and diffuses slowly toward the edge of the lattice. This phenomenon may result in an increase in the slope of the average first-passage time curve at a distance comparable with the average size of the large fluid clusters. The size of the large fluid clusters exhibits strong fluctuations because they may coalesce to form one percolated cluster. This cluster size fluctuation is manifested in the increasing variation of the first-passage time along the first-passage time curve (Figure 4a). Upon further decreasing the temperature, it becomes rare to find a molecule inside a fluid cluster, i.e., a cluster of 14 fluid chains, and in our simulations the sample size is too small to provide a reliable average first-passage time curve.

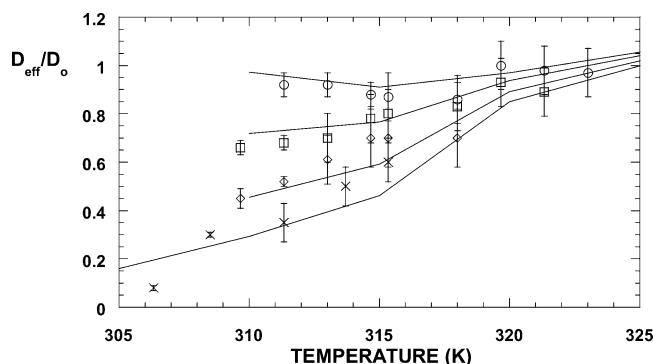


Figure 8. Relative diffusion coefficient. The relative diffusion coefficient, D_{eff}/D_o , of fluid DMPC, measured in a spherical supported equimolar DMPC/DSPC bilayer by 2-D exchange NMR method,⁷⁶ is plotted against the rescaled experimental temperature. By adding 5 °C to the experimental temperatures, we rescaled the temperature in order to make the phase transition properties of a spherical supported bilayer comparable to that of an MLV. The measurements were performed at the following mixing times: 12 ms (leaning cross), 6 ms (diamond), 4 ms (square), 2 ms (circle). Solid lines connect the relative diffusion coefficients calculated at the following simulation temperatures: 305, 310, 315, 320, and 325 K. The curves from the bottom to the top have been calculated at the following rescaled mixing times: 300, 80, 20, and 8 μs . D_{eff} of a DMPC molecule, located initially in a fluid domain of an equimolar DMPC/DSPC bilayer, was calculated using eq 18 and the values of β and α , shown by squares in Figure 5a and Figure 5c, respectively. The diffusion constant of fluid DMPC in a one-component DMPC bilayer (D_o) was calculated according to the following equation: $D_o = A \exp(-E_a/RT)$, where the parameters A and E_a are listed in Table 1. The proportionality factor in eq 18 was chosen to get $D_o = D_{\text{eff}}$ at 325 K, i.e., close to the onset temperature of the fluid-to-gel transition in an equimolar DMPC/DSPC bilayer, and at a rescaled mixing time of $t_{\text{rm}} = 8 \mu\text{s}$. The standard error of the calculated relative diffusion coefficient, $\pm 30\%$ (not shown), is primarily originated from the standard error of D_o (see ref 35).

Comparison with NMR Experiments

Dolainsky et al.⁷⁶ investigated the lateral diffusion of perdeuterated DMPC (DMPC-d9 and DMPC-d54) in a spherical supported equimolar DMPC/DSPC bilayer using two-dimensional exchange and field gradient solid-state NMR methods. They determined the relative diffusion coefficient of DMPC, D_{eff}/D_o , in the fluid regions at different temperatures and mixing times t_m . According to their definition the effective diffusion coefficient is

$$D_{\text{eff}} = \frac{\langle r^2 \rangle}{4t_m} \quad (17)$$

where $\langle r^2 \rangle$ is the average of the square of the radial distance traveled by the fluid state perdeuterated DMPC molecule during time t_m . D_o is the diffusion coefficient of DMPC in the fluid phase of a one-component DMPC bilayer. The NMR measurements were performed in the temperature range of the gel/fluid mixed phase of an equimolar DMPC/DSPC mixture. The observed relative diffusion coefficient is plotted against the temperature in Figure 8, where each symbol belongs to different mixing times. In Figure 8, the experimental temperature is rescaled by adding 5 °C to the experimental temperatures. Rescaling makes the gel-to-fluid transition properties of a spherical supported bilayer comparable to that of a multilamellar vesicle (MLV). At a given temperature and at short enough mixing times, the linear size of the fluid regions is larger than the radial distance traveled by the tracked DMPC molecules and the effective diffusion coefficient D_{eff} is comparable with D_o (see open circles in Figure 8). At longer mixing times,

however, the linear size of the fluid regions is smaller than the radial distance traveled by the tracked DMPC molecule. In this case the tracked molecule may visit a gel/fluid interface or become part of a gel cluster, where the diffusion step takes longer and D_{eff} becomes smaller. By decreasing the temperature, the linear size of the fluid regions becomes smaller, resulting in further decreases to D_{eff} .

To compare the experimental data with the results of our simulations we have taken into consideration that the experimental length scale, from 0.1 to 1 μm , is 2–3 orders of magnitude greater than the length scale of the simulations. Because of this length scale difference, we rescaled the mixing times and calculated the effective diffusion coefficient from the simulated data as follows:

$$D_{\text{eff}} \propto \frac{\lambda^2}{4t_{\text{rm}}} \left(\frac{t_{\text{rm}}}{\alpha} \right)^{2/\beta} \quad (18)$$

where eq 18 is obtained after substituting eq 13 into eq 17, t_{rm} is the rescaled mixing time, and the values of α and β for the fluid DMPC molecules are given by the squares in Figure 5a and Figure 5c, respectively. The diffusion coefficient of DMPC in the fluid phase can be calculated according to the Arrhenius equation (see the legend to Table 1).

The best agreement between the simulated and experimental relative diffusion coefficient can be obtained by rescaling the experimental mixing times: $t_m = 12, 6, 4$, and 2 ms to $t_{\text{rm}} = 300, 80, 20$, and $\leq 8 \mu\text{s}$, respectively. There is a linear relationship between t_m and t_{rm} for all but the shortest mixing time. At the shortest mixing time, 2 ms, $D_{\text{eff}} \approx D_o$ at every experimental temperature, and any rescaled mixing time below 8 μs results in a good fit. In Figure 8, solid lines show the calculated relative diffusion coefficient vs temperature curves at different rescaled mixing times. The standard error of each calculated relative diffusion coefficient is $\pm 30\%$, primarily originated from the standard error of D_o (see ref 35). The calculated values agree with the NMR data within experimental error. The relative diffusion coefficient continuously decreases with the temperature in the fluid/gel mixed phase region of the phase diagram, and the rate of the decrease tends to be larger with increasing mixing time. Thus, in contrast to the FRAP probe molecules, there is no threshold temperature for the long-range diffusion of intrinsic molecules that may exist in either fluid or gel phase regions.

Conclusions

According to the raft hypothesis, lateral heterogeneity of the membrane components has profound effects on functions of the cell such as signal transduction.⁷⁷ In this paper the effect of membrane heterogeneity on the lateral diffusion of intrinsic membrane lipids is demonstrated. The lateral diffusion of the intrinsic molecules in an equimolar DMPC/DSPC mixture has been simulated by a thoroughly tested two-state model of two-component phospholipid bilayers. The components are involved in normal diffusion in the extreme gel and fluid phase regions. In these regions the components are randomly distributed. In the gel/fluid and gel/gel mixed phase regions, however, there are deviations from normal diffusion. In these mixed phase regions the distribution of the components deviates from random distribution. In the gel/fluid mixed phase region the diffusion of components situated initially inside a fluid cluster is slower than in the extreme fluid phase region (sub-diffusion). The diffusion of a DMPC molecule, situated initially inside a gel cluster, is faster than that of a DMPC molecule in the extreme

gel phase region (super-diffusion). The diffusion of intrinsic molecules is anomalous, but not because of a specific diffusion mechanism. The possibility of anomalous diffusion in membranes arises because the diffusing molecule visits a variety of different environments characterized by its relative proximity to various membrane components. However, this is not sufficient for anomalous diffusion; e.g., in the extreme gel and fluid phase regions of DMPC/DSPC mixtures the diffusion is normal. The diffusion is actually anomalous because the components of the bilayer are nonrandomly distributed. The deviation from random distribution is strongly correlated by β .

Similar to the results of the NMR experiments, the calculated relative diffusion coefficient continuously decreases in the gel/fluid mixed phase region with decreasing temperature. There is no threshold temperature for the long-range diffusion of intrinsic molecules, because they can enter into gel phase regions. In contrast, FRAP probe molecule partitions exclusively into the fluid phase and its long-range diffusion is blocked with the percolation of the gel clusters. However, above the percolation threshold temperature of gel clusters and below the liquidus curve the FRAP probe molecules are expected to show long-range anomalous subdiffusion, because in this region the fluid phase is connected and the distribution of the components is not random. This prediction could be experimentally tested.

Acknowledgment. We thank Professor Thomas Heimburg and Heiko Seeger (Niels Bohr Institute) for sharing the fluorescence correlation spectroscopy data on DMPC and DSPC bilayers. This work was supported by grants from the NIH (GM 59205 to R.L.B.) and from Pfizer Inc. (to I.P.S.). I.P.S. acknowledges Mrs. Lawrence Garner's generous support. I.P.S. is also grateful to Professor Thomas E. Thompson for the discussions in 1987 on lipid lateral diffusion, initiating this paper.

Appendix 1

In thermal equilibrium, $dP_i/dt = 0$ for every i configuration and the detailed balance, i.e.,

$$k_{i \rightarrow j} P_i^{\text{eq}} = k_{j \rightarrow i} P_j^{\text{eq}} \quad (19)$$

for every i - j pair of configurations can be (in most cases) derived.⁷⁸ By means of the detailed balance conditions, one can derive a general form for the transition frequencies. After substituting eq 8 into eq 19 we get

$$\frac{k_{i \rightarrow j}}{k_{j \rightarrow i}} = \frac{P_j^{\text{eq}}}{P_i^{\text{eq}}} = \frac{e^{-E_j/kT}}{e^{-E_i/kT}} = \frac{e^{(E_i - E_j)/2kT}}{e^{(E_j - E_i)/2kT}} \quad (20)$$

Thus the transition frequencies can be calculated as follows:

$$\begin{aligned} k_{i \rightarrow j} &= v_{ij}(T) e^{(E_i - E_j)/2kT} \\ k_{j \rightarrow i} &= v_{ji}(T) e^{(E_j - E_i)/2kT} \end{aligned} \quad (21)$$

where the proportionality factors should be equal to each other, i.e., $v_{ij}(T) \equiv v_{ji}(T)$.

Appendix 2

By analyzing the size distributions of DMPC and DSPC clusters at different temperatures and mole fractions one can construct the heavy solid lines in Figure 7. To get one point of the left-hand side heavy line we keep the simulation temperature constant and gradually decrease the DSPC mole fraction from

50%. At this mole fraction the size distribution of DSPC clusters is bimodal. The cusp-like peak at small cluster sizes refers to the numerous small DSPC clusters, most of which contain only one DSPC molecule. The second peak of the distribution is related to the size distribution of the largest DSPC cluster at each snapshot.⁵⁶ With decreasing DSPC mole fractions, the second peak gets closer to the first peak and they overlap with each other more and more. At a certain temperature the second peak disappears, the distribution becomes unimodal, and only the shoulder of the cusp-like peak signifies that the respective cluster size population is inhomogeneous. Further decreasing the DSPC mole fraction causes even the shoulder to disappear. This is the percolation threshold concentration of DSPC clusters, and it is plotted on the temperature-mole fraction plane as part of the left-hand side heavy solid line. At the percolation threshold the population of the cluster size changes from inhomogeneous to homogeneous.

In the inhomogeneous population, the size of the largest cluster increases with increasing system size while the rest of the clusters remain small. In a homogeneous population, however, every cluster remains small with increasing system size.

In Figure 7 the heavy solid line on the right-hand side was similarly generated by analyzing the size distribution of the DMPC clusters. The line gives the percolation threshold concentration of DMPC clusters at every temperature.

The construction of the dash-dotted lines was similar to that of the heavy solid lines, but we used a modified version of the DMPC/DSPC model. We changed the parameter values of the original DMPC/DSPC model by selecting the same E_{jk}^{mm} interaction energies for every chain-chain interaction. With this choice of the energy parameters there is no energetic preference for the nearest neighbors of a chain and thus the lateral distribution of the components is random at every temperature and mole fraction. At a constant temperature we gradually decrease the DSPC mole fraction from 50% and investigate the cluster size distribution. Before the percolation threshold DSPC mole fraction, given by the left dash-dotted line in Figure 7, the peaks of the bimodal size distribution of the DSPC clusters overlap with each other more and more. At the threshold, even the remnants of the second peak disappear.

The DSPC cluster size distributions generated from the original and the modified model are similar below the percolation threshold of DSPC mole fraction of the original model. Thus, before reaching the left-hand side heavy solid line (in Figure 7) the distribution of the components in the original model is random. The DMPC cluster size distributions generated from the original and the modified model are similar below the percolation threshold of DMPC mole fraction of the original model. Thus before reaching the right-hand side heavy solid line (in Figure 7) the distribution of the components in the original model is random. Between the two heavy solid lines, however, the cluster size distributions of the original and modified models deviate from each other, and thus the distribution of the components of the original model is not random, i.e.: the distribution is correlated.

There are two dashed lines in Figure 7, the one at the higher temperatures is called the liquidus curve and the one at the lower temperatures is called the solidus curve. These dashed lines were constructed from the calculated excess heat capacity curves. At a given mole fraction, the excess heat capacity curve is the temperature derivative of the average membrane energy vs temperature curve. The excess heat capacity is sharply rising from the onset temperature of the gel-to-fluid transition and

sharply falling before the completion of the transition. The onset temperature is defined by the intercept of the zero line and the straight line fitted to the initial inflection point of the excess heat capacity curve. The solidus and liquidus curve is constructed from the onset and completion temperatures, respectively, determined at different mole fractions.

References and Notes

- (1) Lenaz, G. *J. Membr. Biol.* **1988**, *104*, 193–209.
- (2) Hackenbrock, C. R.; Chazotte, B.; Gupte, S. S. *J. Bioenerg. Biomembr.* **1986**, *18*, 331–368.
- (3) Lavergne, J.; Joliot, P. *Trends Biochem. Sci.* **1991**, *16*, 129–134.
- (4) McCloskey, M. A.; Poo, M.-m. *J. Cell Biol.* **1986**, *102*, 2185–2196.
- (5) Chan, P.-Y.; Lawrence, M. B.; Dustin, M. L.; Ferguson, L. M.; Golan, D. E.; Springer, T. A. *J. Cell Biol.* **1991**, *115*, 245–255.
- (6) Dustin, M. L.; Ferguson, L. M.; Chan, P.-Y.; Springer, T. A.; Golan, D. E. *J. Cell Biol.* **1996**, *132*, 465–474.
- (7) Metzger, H.; Kinet, J.-P. *FASEB J.* **1988**, *2*, 3–11.
- (8) Holowka, D.; Baird, B. *Annu. Rev. Biophys. Biomol. Struct.* **1996**, *25*, 79–112.
- (9) Schlessinger, J. *Trends Biochem. Sci.* **1980**, *5*, 210–214.
- (10) Schlessinger, J. *Harvey Lect.* **1993–1994**, *89*, 105–123.
- (11) Heldin, C. H. *Cell* **1995**, *80*, 213–223.
- (12) Tocane, J.-F.; Dupou-Cezanne, L.; Lopez, A. *Prog. Lipid. Res.* **1994**, *33*, 203–237.
- (13) Saxton, M. J. *Curr. Top. Membr.* **1999**, *48*, 229–282.
- (14) Shin, Y.-K.; Ewert, U.; Budil, D. E.; Freed, J. H. *Biophys. J.* **1991**, *59*, 950–957.
- (15) Freed, J. H. *Annu. Rev. Biophys. Biomol. Struct.* **1994**, *23*, 1–25.
- (16) Galla, H. J.; Hartmann, W.; Theilen, U.; Sackmann, E. *J. Membr. Biol.* **1979**, *48*, 215–236.
- (17) Sassaroli, M.; Vauhkonen, M.; Perry, D.; Eisinger, J. *Biophys. J.* **1990**, *57*, 281–290.
- (18) Davenport, L. Fluorescence probes for studying membrane heterogeneity. In *Methods in Enzymology*; Brand, L., Johnson, M. L., Eds.; Academic Press: San Diego, 1997; Vol. 278, pp 487–512.
- (19) Terpetsching, E.; Szmancinski, H.; Lakowicz, J. R. Long-lifetime metal–ligand complexes as probes in biophysics and clinical chemistry. In *Methods in Enzymology*; Brand, L., Johnson, M. L., Eds.; Academic Press: San Diego, 1997; Vol. 278, pp 295–321.
- (20) Vaz, W. L. C.; Derzko, Z. I.; Jacobson, K. A. *Cell Surf. Rev.* **1982**, *8*, 83–136.
- (21) Vaz, W. L. C.; Melo, E. C. C.; Thompson, T. E. *Biophys. J.* **1989**, *56*, 869–876.
- (22) Kapiza, H. G.; Ruppel, D. A.; Galla, H.-J.; Sackmann, E. *Biophys. J.* **1984**, *45*, 577–587.
- (23) Tamm, L. K. *Biochemistry* **1988**, *27*, 1450–1457.
- (24) Saxton, M. J.; Jacobson, K. *Annu. Rev. Biophys. Biomol. Struct.* **1997**, *26*, 373–399.
- (25) Matko, J.; Edidin, M. Energy transfer methods for detecting molecular clusters on cell surfaces. In *Methods in Enzymology*; Brand, L., Johnson, M. L., Eds.; Academic Press: San Diego, 1997; Vol. 278, pp 444–462.
- (26) Wu, P.; Brand, L. *Annal. Biochem.* **1994**, *218*, 1–13.
- (27) Petersen, N. O.; Hoddellius, P. L.; Wiseman, P. W.; Seger, O.; Magnusson, K.-E. *Biophys. J.* **1993**, *65*, 1135–1146.
- (28) Huang, Z.; Thompson, N. L. *Biophys. J.* **1996**, *70*, 2001–2007.
- (29) Svoboda, K.; Block, S. M. *Annu. Rev. Biophys. Biomol. Struct.* **1994**, *23*, 247–285.
- (30) Sheetz, M. P. *Methods Cell Biol.* **1998**; Vol. 55.
- (31) Edidin, M.; Kuo, S. C.; Sheetz, M. P. *Science* **1991**, *254*, 1379–1382.
- (32) Edidin, M.; Zuniga, M. C.; Sheetz, M. P. *Proc. Natl. Acad. Sci. U.S.A.* **1994**, *91*, 3378–3382.
- (33) Kusumi, A.; Sako, Y.; Fujiwara, T.; Tomishige, M. *Methods Cell Biol.* **1998**, *55*, 173–194.
- (34) König, S.; Pfeiffer, W.; Bayerl, T.; Richter, D.; Sackmann, E. *J. Phys.* **1992**, *II 2*, 1589–1615.
- (35) Kuo, A.-L.; Wade, C. G. *Biochemistry* **1979**, *18*, 2300–2308.
- (36) Crawford, M. S.; Gerstein, B. C.; Kuo, A.-L.; Wade, C. G. *J. Am. Chem. Soc.* **1980**, *102*, 3728–3732.
- (37) Stauffer, D.; Aharony, A. *Introduction to Percolation Theory*, 2nd ed.; Frances and Taylor: London, 1992.
- (38) Bouchard, J. P.; Georges, A. *Phys. Rep.* **1990**, *195*, 127–293.
- (39) Eisinger, J.; Flores, J.; Petersen, W. P. *Biophys. J.* **1986**, *49*, 987–1001.
- (40) Saxton, M. J. *Biophys. J.* **1993**, *64*, 1053–1062.
- (41) Schram, V.; Lin, H.-N.; Thompson, T. E. *Biophys. J.* **1996**, *71*, 1811–1822.
- (42) Saxton, M. J. *Biophys. J.* **1982**, *39*, 165–173.
- (43) Torquato, S. *Appl. Mech. Rev.* **1991**, *44*, 37–76.
- (44) Torquato, S. *Physica A (Amsterdam)* **1994**, *207*, 70–91.
- (45) Almeida, P. F. F.; Vaz, W. L. C.; Thompson, T. E. *Biochemistry* **1992**, *31*, 6739–6747.
- (46) Pink, D. A.; Green, T. J.; Chapman, D. *Biochemistry* **1980**, *19*, 349–357.
- (47) Jorgensen, K.; Sperotto, M. M.; Mouritsen, O. G.; Ipsen, J. H.; Zuckermann, M. J. *Biochim. Biophys. Acta* **1993**, *1152*, 135–145.
- (48) Jorgensen, K.; Klinger, A.; Braiman, M.; Biltonen, R. L. *J. Phys. Chem.* **1996**, *100*, 2766–2769.
- (49) Jorgensen, K.; Klinger, A.; Biltonen, R. L. *J. Phys. Chem.* **2000**, *104*, 11763–11773.
- (50) Jorgensen, K.; Mouritsen, O. G. *Biophys. J.* **1995**, *95*, 942–954.
- (51) Sugar, I. P.; Biltonen, R. L.; Mitchard, N. Monte Carlo simulations of membranes: The phase transition of small unilamellar DPPC vesicles. In *Methods in Enzymology*; 1994; Vol. 240, pp 569–593.
- (52) Sugar, I. P.; Thompson, T. E.; Biltonen, R. L. *Biophys. J.* **1999**, *76*, 2099–2110.
- (53) Michonova-Alexova, E. I.; Sugar, I. P. *Biophys. J.* **2002**, *83*, 1820–1833.
- (54) Sugar, I. P.; Biltonen, R. L. Structure–function relationships in two-component phospholipid bilayers. A Monte Carlo simulation approach using a two-state model. In *Methods in Enzymology*; 2000; Vol. 323, pp 340–372.
- (55) Sugar, I. P.; Michonova-Alexova, E.; Chong, P., L.-G. *Biophys. J.* **2001**, *81*, 2425–2441.
- (56) Michonova-Alexova, E. I.; Sugar, I. P. *J. Phys. Chem. B* **2001**, *105*, 10076–10083.
- (57) Janiak, M. J.; Small, D. M.; Shipley, G. G. *J. Biol. Chem.* **1979**, *254*, 6068–6078.
- (58) Hui, S. W.; Viswanathan, R.; Zasadzinski, J. A.; Israelachvili, J. N. *Biophys. J.* **1995**, *68*, 171–178.
- (59) Huang, K. *Statistical Mechanics*; Wiley: New York, 1963; p. 336.
- (60) Metropolis, M.; Rosenbluth, A. W.; Rosenbluth, M. N.; Teller, A. N. *J. Chem. Phys.* **1953**, *21*, 1087–1092.
- (61) Sun, H.; Sugar, I. P. *J. Phys. Chem. B* **1997**, *101*, 3221–3227.
- (62) Hac, A. E.; Seeger, H. M.; Fidorra, M.; Heimbürg, T. *Biophys. J.* **2005**, *88*, 317–333.
- (63) Hac, A.; Seeger, H.; Heimbürg, T. *Biophys. J.* **2003**, *84*, 326a.
- (64) Weaver, D. L. *Biophys. J.* **1982**, *38*, 311–313.
- (65) Smith, B. A.; McConnell, H. M. *Proc. Natl. Acad. Sci. U.S.A.* **1978**, *75*, 2759–2763.
- (66) Cohen, M. H.; Turnbull, D. *J. Chem. Phys.* **1959**, *31*, 1164–1169.
- (67) Vaz, W. L. C.; Clegg, R. M.; Hallmann, D. *Biochemistry* **1985**, *24*, 781–786.
- (68) MacCarthy, J.; Kozak, J. *J. Chem. Phys.* **1977**, *77*, 2214–2216.
- (69) Nagle, J. F.; Wilkinson, D. A. *Biophys. J.* **1982**, *23*, 159–175.
- (70) Scher, H.; Shlesinger, M. F.; Bendler, J. T. *Phys. Today* **1991**, 26–34.
- (71) Nagle, J. F. *Biophys. J.* **1992**, *63*, 366–370.
- (72) Knoll, W.; Ibel, K.; Sackmann, E. *Biochemistry* **1981**, *20*, 6379–6383.
- (73) Knoll, W.; Schmidt, G.; Sackmann, E.; Ibel, K. *J. Chem. Phys.* **1983**, *79*, 3439–3442.
- (74) Waner, S. On line program for multivariate regression analysis is at http://people.hofstra.edu/faculty/Stefan_Waner/RealWorld/multinreg.html.
- (75) Weisstein, E. W. Random Walk–2-Dimensional. From *MathWorld*—A Wolfram Web Resource. <http://mathworld.wolfram.com/RandomWalk2-Dimensional.html>
- (76) Dolainsky, C.; Karakatsanis, P.; Bayerl, T. M. *Phys. Rev. E* **1997**, *55*, 4512–4521.
- (77) Simons, K.; Toomre, D. *Nat. Rev. Mol. Cell Biol.* **2000**, *1*, 31–39.
- (78) Haken, H. In *Synergetics*; Springer-Verlag: Berlin, 1983; p 89.